Computational modelling of coupled dynamic phase transformations in shape memory alloys

Mahapatra, D. R. and Melnik, R.V.N.

In: Proceedings of the 19th International Symposium on High Performance Computing Systems and Applications, HPCS-2005, IEEE pp. 267--273, 2005.

DOI Bookmark:10.1109/HPCS.2005.21

Proceedings

19th International Symposium on High Performance Computing Systems and Applications

---

HPCS 2005

Proceedings

19th International Symposium on High Performance Computing Systems and Applications

HPCS 2005

15-18 May 2005
Guelph, Ontario Canada

Sponsored by

C3.ca ♦ SUN Microsystems of Canada ♦ IBM Canada ♦ SGI Canada ♦ HP Canada ♦ NORTEL ♦ ORION ♦ Cray Inc. ♦ FORCE 10 Networks ♦ Platform Computing ♦ Audcomp Computer Systems ♦ HECMS ♦ ACEnet ♦ SHARCNET

IEEE
COMPUTER
SOCIETY

IEEE

Los Alamitos, California
Washington • Brussels • Tokyo

Computational modeling of coupled dynamic phase transformations in shape memory alloys

D. Roy Mahapatra and R.V.N. Melnik
Mathematical Modelling and Computational Sciences,
Wilfrid Laurier University, 75 University Avenue West,
Waterloo, Ontario, Canada N2L 3C5
Email: droymahapatra@wlu.ca, rmelnik@wlu.ca

Abstract

In spite of several modeling approaches to understand the shape memory alloy (SMA) behaviour, many difficulties exist because of the various limitations of the existing free energy models. Associated phase kinetics coupled with the thermoelstodynamics is still not fully tractable. A new dynamic model of 3D SMA is developed in this paper which employs an improved version of the microscopic Landau theory. Essential properties of the single and multivariant martensitic phase transformations are recovered using consistent steps, which eliminates the problem of nonuniqueness of energy partitioning and relaxes the oversensitivity of the free energy due to many unknown material constants in previously reported models. The newly developed microscopic model is incorporate in a variationally formulated finite element framework. Newmark's time integration scheme is adopted and the condition for consistent iteration to solve the strongly nonlinear system at each time step is highlighted. Banded assembly of the discretized system matrix is performed in parallel. A parallel PCG method with Jacobi preconditioner is employed to solve the system at each time step.

1. Introduction

Dynamics of phase transformation (PT) in Shape Memory Alloys (SMAs) under the combined effect of stress and temperature is one of the most complex and intriguing phenomena, which is far from being completely tractable till date. Understanding such dynamics with the aid of multiphysics multiscale computational model is important in order to design new materials and devices by harnessing the shape memory effect. Phenomenological framework based on Landau theory of martensitic transformation has become a convenient choice of basic building block in the computational models. However, most of the phenomenological models are applicable in macroscopic and mesoscopic scales as discussed in [10]. A macroscopic model requires the description of the 3D geometry and variational minimization of an appropriate potential involving the thermoelastic energy and the energy due to dynamic self-accommodation of the martensitic variants. Whereas a mesoscopic model, such as the Falk-Kanopka free energy model [3], requires the description of the free energy as a function of the strain invariants of a single crystal and its point group symmetry.

In the present paper we report a newly developed microscopic free energy function and the associated coupled field model to simulate the dynamics of 3D macroscopic sample. A 3D model similar to those reported in [6, 7] is developed in this paper. It is observed from the study in [7] that the free energy is highly sensitive to many interdependent constants which are to be obtained experimentally. As a result of this sensitivity and due to a fairly complex polynomial representation of the 3D Landau-Ginzburg free energy function, there may be situations where multidimensional simulations produce unphysical spurious oscillations. In the new model developed in the present paper, the above set of interdependent constants is reduced to uniquely identifiable set of constants for each transformation surface among the austenitic phase and a particular martensitic variant. However, in order to complete the description of such model, the value of the spontaneous strains are to be estimated from a molecular dynamics simulation as done in [7] in a decoupled manner. Coupling such a molecular dynamic model is another involved task and is not attempted in the present work.

Based on the general Falk-Kanopka free energy representation in [10] a new low-dimensional model for the time-dependent dynamics of SMA was derived. A rigorous numerical analysis of a class of such reduced models was carried out in [9] and computational results obtained with such models confirmed their robustness for a number of practically important cases. Very few and simplified studies are

Proceedings of the 19th International Symposium on High Performance Computing Systems and Applications (HPCS'05)
1550-5243/05 $20.00 © 2005 IEEE

available (e.g. [4, 8]) where the time-dependent Ginzburg-Landau (TDGL) (Langevin) equation with the correct microscopic description of the Falk-Kanopka type free energy function has been solved. We are not aware of any dynamic model of 3D SMA samples that bases its consideration on the correct Ginzburg-Landau free energy representation in the microscopic scale and the momentum balance and heat conduction in the macroscopic scale. The Ginzburg-Landau free energy function derived in the first part of this paper is incorporated in the coupled field model. A special case of cubic to tetragonal PT with single martensitic variant along the axis of a bar with rectangular cross-section under axial stress and heat flux is analyzed to check the performance of the model. Finally, a variational formulation is reported for the general case, which is then followed by finite element (FE) discretization scheme for parallel computer implementation.

In order to perform the time-dependent study of real SMA device having complex geometry in three-dimension, it is essential to develop efficient and large-scale computational scheme based on the proposed mathematical model. The reason for the large size of the computational model is because of the requirement that the microstructural morphology of the SMA needs to be represented accurately. Therefore, one requires FE mesh with its element size in the order of microns and discretize a total volume which is at least in the order of centimeters. The reason for computation intensiveness of the time-dependent dynamics is because of the fact that there are combined effects of various time scales (i.e. the loading rate, the velocities of thermoelastic wave and phonon propagation, rate kinetics of the PT etc.). However, till date there is no robust mathematical model and well-defined steps reported in published literature which can deal with general time-dependent dynamics of SMA. A majority of the computational modelling and simulations to analyze the phase transformation in SMA is based on use of commercial FE packages [13, 11]. Here, one typically needs to specify the material constitutive model for spatial integration at the element level. Although a volume averaged constitutive properties of a particular phase can be prescribed, the evolution of the phase boundaries are not possible to track in this manner. Also the actual coupling between the thermoelasticity and the transformation kinetics are absent in such model. Therefore, implementation of a coupled FE model and consistent non-uniform time stepping scheme in a parallel computational environment is an essential but a challenging task.

2. 3D Landau theory of martensitic phase transformation

It has been demonstrated by Levitas and Preston [6, 8] that the polynomial structures 2-3-4 and 2-4-6 of of the Gibbs free energy in order parameter η in Cartesian coordinate can eliminate the problem of unphysical minima and retain all the necessary properties of the Ginzburg-Landau free energy function with respect to point group symmetry of the crystals. Also such polynomial structure can be made in such a way that the stability of the austenitic phase (A) and martensitic variants (M_j), non-extremal diffusion barrier and nucleation can be described in stress-temperature space. Also, while using such polynomial structure the interfaces (domain walls) $M_j - M_i$ between the martensitic variants (i, j) can be interpreted by using a newly introduced barrierless A nucleation mechanism, i.e. by splitting the original into two simultaneously present interfaces $M_j - A$ and $A - M_i$. In this section a 2-3-4 polynomial structure is constructed by improving upon the model of Levitas and Preston [6, 7].

For analytical clarity we first consider a single variant of martensite and single order parameter $\eta \in [0, 1]$. First we define the Gibbs free energy density in stress-temperature space $(\boldsymbol{\sigma}, \theta)$ as

$$G = -\boldsymbol{\sigma} : \boldsymbol{\lambda} : \boldsymbol{\sigma}/2 - \boldsymbol{\sigma} : \boldsymbol{\varepsilon}_t \varphi(\eta) + f(\theta, \eta) \ , \qquad (1)$$

where $\boldsymbol{\lambda}$ is the constant fourth-rank elastic compliance tensor, $\boldsymbol{\varepsilon}_t$ is the transformation strain tensor at the thermodynamic equilibrium of the martensite (obtained from crystallography), $\varphi(\eta)$ is a monotonic function with $\varphi(0) = 0$ indicating stable A phase and $\varphi(1) = 1$ indicating stable M phase. $f(\theta, \eta)$ is the chemical part of the energy with property: $f(\theta, 1) - f(\theta, 0) = \Delta G^{\theta}(\theta)$, where ΔG^{θ} is the difference between the thermal parts of the Gibbs free energy density of the M and A phases, which can be obtained indirectly from experiments through the relation [14]

$$\Delta G^{\theta} = -\Delta s_e(\theta - \theta_e) - \Delta c\theta \left[\ln(\theta/\theta_e) - 1\right] - \Delta c\theta_e \ , \ (2)$$

where Δc is the difference between the specific heat of the phases, Δs_e is the jump in the specific entropy at the equilibrium temperature (θ_e). The objective is to obtain the functions φ and f by satisfying their properties mentioned above and the conditions of extremum of the energy for existence of equilibrium of A and M phases: $\partial G/\partial \eta = 0$ at $\eta = 0, 1$.

The new model derived below is based on the assumption that G can be uniquely represented by a polynomial structure in η with the extremum only at $\eta = 0, 1$ and out of these two extremum only one is minimum and the other is maximum for phase transformation (PT) to happen. At equilibrium

$$\frac{\partial G}{\partial \eta} = -\boldsymbol{\sigma} : \boldsymbol{\varepsilon}_t \frac{\partial \varphi(\eta)}{\partial \eta} + \frac{\partial f(\theta, \eta)}{\partial \eta} = 0 \ , \quad \eta = 0, 1 \quad (3)$$

The total strain tensor ($\boldsymbol{\varepsilon} = -\partial G/\partial \boldsymbol{\sigma}$) is the sum of the elastic strain tensor ($\boldsymbol{\lambda} : \boldsymbol{\sigma}$) and the transformation strain tensor ($\boldsymbol{\varepsilon}_t \varphi(\eta)$). Hence for reconstructive PT through vanishing misfit strain, the condition

$$\boldsymbol{\sigma} : \boldsymbol{\varepsilon}_t \frac{\partial \varphi(\eta)}{\partial \boldsymbol{\sigma}} - \frac{f(\theta,\eta)}{\partial \boldsymbol{\sigma}} = 0 \quad \forall(\boldsymbol{\sigma},\eta) \tag{4}$$

must be satisfied. It is observed in the reported results [6] that the transformation barrier is dependent on stress. In the context of interface barrier, Levitas and Preston [8] have treated the associated η to be dependent on $\boldsymbol{\sigma}$. In the present paper, we propose an alternate approach by considering stress-dependent barrier height because the stress $\boldsymbol{\sigma}$ is the only driving factor for PT under isothermal condition. The polynomial structure which satisfies the extremum properties can be expressed as

$$\frac{\partial G}{\partial \eta} = \eta(\eta-1)(\eta-\eta_b) \ , \tag{5}$$

so that its roots $\eta = 0, 1$ satisfy Eq. (3) and the root $\eta = \eta_b(\boldsymbol{\sigma},\theta)$ represents the $A \leftrightarrow M$ PT barrier. Integrating Eq. (5) and imposing the combined properties of $\varphi(\eta)$ and $f(\theta,\eta)$ stated earlier as

$$G(\boldsymbol{\sigma},\theta,0) - G(\boldsymbol{\sigma},\theta,1) = \boldsymbol{\sigma} : \boldsymbol{\varepsilon}_t - \Delta G^\theta \ , \tag{6}$$

we get

$$\eta_b = -6\boldsymbol{\sigma} : \boldsymbol{\varepsilon}_t + 6\Delta G^\theta + 1/2 \ . \tag{7}$$

Using Eq. (1) in Eq. (5) and by differentiating with respect to $\boldsymbol{\sigma}$, one has

$$-\boldsymbol{\varepsilon}_t \frac{\partial \varphi(\eta)}{\partial \eta} - \boldsymbol{\sigma} : \boldsymbol{\varepsilon}_t \frac{\partial^2 \varphi(\eta)}{\partial \boldsymbol{\sigma} \partial \eta} + \frac{\partial^2 f(\theta,\eta)}{\partial \boldsymbol{\sigma} \partial \eta}$$

$$= \frac{\partial}{\partial \boldsymbol{\sigma}} \left[\eta_b \eta - (\eta_b+1)\eta^2 + \eta^3 \right] \ . \tag{8}$$

The term involving f can be eliminated from Eq. (8) with the help of Eq. (4), and can be expressed as

$$\boldsymbol{\varepsilon}_t \frac{\partial \varphi(\eta)}{\partial \eta} = \eta(\eta-1)\frac{\partial \eta_b}{\partial \boldsymbol{\sigma}} = \eta(\eta-1)(-6\boldsymbol{\varepsilon}_t) \ . \tag{9}$$

Integrating Eq. (9) and following the properties of the transformation strain, i.e. $\varphi(0) = 0$ and $\varphi(1) = 1$,

$$\varphi(\eta) = 3\eta^2 - 2\eta^3 \ , \quad 0 \leq \eta \leq 1 \ , \tag{10}$$

Substituting this form in Eq. (4) and integrating with respect to η, the chemical part of the free energy density is obtained as

$$f(\theta,\eta) = \boldsymbol{\sigma} : \boldsymbol{\varepsilon}_t(3\eta^2 - 2\eta^3) + \frac{1}{2}\eta_b\eta^2 - \frac{1}{3}(\eta_b+1)\eta^3 + \frac{1}{4}\eta^4 \ . \tag{11}$$

For $A \rightarrow M$ PT, the criteria for the loss of stability of A phase is $\partial^2 G/\partial \eta^2 \leq 0$ at $\eta = 0$, which gives the stress driven condition:

$$\boldsymbol{\sigma} : \boldsymbol{\varepsilon}_t \geq \Delta G^\theta + \frac{1}{12} \ . \tag{12}$$

Similarly, for $M \rightarrow A$ PT, the criteria for the loss of stability is $\partial^2 G/\partial \eta^2 \leq 0$ at $\eta = 1$, which gives the stress driven condition:

$$\boldsymbol{\sigma} : \boldsymbol{\varepsilon}_t \leq \Delta G^\theta - \frac{1}{12} \ . \tag{13}$$

$M_j \leftrightarrow M_i$ PT or diffused interface can evolve for stresses outside the range obtained by Eqs. (12) and (13). Note that no parameter fitting is required in the present model as opposed to the earlier model [6].

2.1. Cubic to tetragonal transformation characteristics

We now consider the cubic to tetragonal PT for single variant martensitic case in absence of the elastic part of the stress. In the Cartesian reference frame $(\boldsymbol{e}_1, \boldsymbol{e}_2, \boldsymbol{e}_3)$, the strain and the stress tensors are given by

$$\boldsymbol{\varepsilon}_t = \varepsilon(\boldsymbol{e}_1\boldsymbol{e}_2 - \frac{1}{2}\boldsymbol{e}_2\boldsymbol{e}_2 - \frac{1}{2}\boldsymbol{e}_3\boldsymbol{e}_3) \ , \quad \varepsilon_t = \varepsilon \ ,$$

$$\sigma = \boldsymbol{e}_1.\boldsymbol{\sigma}.\boldsymbol{e}_1 - \frac{1}{2}\boldsymbol{e}_2.\boldsymbol{\sigma}.\boldsymbol{e}_2 - \frac{1}{2}\boldsymbol{e}_3.\boldsymbol{\sigma}.\boldsymbol{e}_3 \ , \quad \sigma_{11} = \sigma_0 \ . \tag{14}$$

Under the uniaxial stress, the equilibrium stress-transformation curve is then described by

$$\eta = \eta_b \Rightarrow \sigma = \frac{1}{\varepsilon_t}\left[\Delta G^\theta + \frac{1-2\eta}{12}\right] \ . \tag{15}$$

Note that the increase in η causes decrease in σ which is consistent. The stress hysteresis (H) is obtained as

$$H = \sigma_{(\eta=0)} - \sigma_{(\eta=1)} = \frac{1}{6\varepsilon_t} \ , \tag{16}$$

which is independent of the temperature. Eq. (15) also shows nonzero tangent moduli where A and M lose their stability. These observations coincide with the results from the earlier model [6].

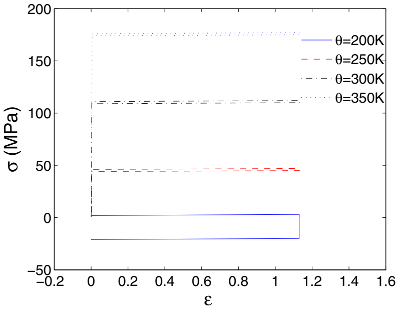

Figure 1. Stress induced transformation characteristics in NiAl under static condition and various temperature state. Equilibrium temperature $\theta^e = 215K$.

Fig. 1 shows the stress induced phase transformation characteristics of NiAl simulated under assumed spontespontaneous $\eta = 0$ (A→M) during loading to $\eta = 1$ (M→A) during unloading. Material properties for single variant martensitic properties are considered, which were used in [7]. This results indicated that the propsoproposed is able to capture the stress hysteresis resonable well without the use of any additional material constants from phenomenological observations.

3. Multivariant phase transformation

In order to model realistic situations and macroscopic sample of SMA it is essential to incorporate the effects of (1) martensitic variants (M_k) (2) thermal strain (3) unequal compliances across the interfaces and the resulting inhomogeneity. For cubic to tetragonal transformation there are three variants of martensite according to the point group of crystallographic symmetry. The Gibbs free energy density thus should poses the associated invariance properties. In the mathematical model, this can be cross-checked by interchanging the variant indices (k). In this paper we consider the same order of variation in the compliance tensor and the thermal expansion tensor as in $\varphi(\eta)$ derived in Sec. 2. The Gibbs free energy density for cubic-tetragonal transformation having three variants $k = 1, 2, 3$ is expressed as

$$G = -\boldsymbol{\sigma} : \left[\boldsymbol{\lambda}_0 + \sum_{k=1}^{3}(\boldsymbol{\lambda}_k - \boldsymbol{\lambda}_0)\varphi(\eta_k)\right] : \boldsymbol{\sigma}/2 - \boldsymbol{\sigma} : \sum_{k=1}^{3}\boldsymbol{\varepsilon}_{tk}\varphi(\eta_k) - \boldsymbol{\sigma} : \left[\boldsymbol{\varepsilon}_{\theta 0} + \sum_{k=1}^{3}(\boldsymbol{\varepsilon}_{\theta k} - \boldsymbol{\varepsilon}_{\theta 0})\varphi(\eta_k)\right] + \sum_{k=1}^{3} f(\theta, \eta_k) + \sum_{i=1}^{2}\sum_{j=i+1}^{3} F_{ij}(\eta_i, \eta_j) \;, \quad (17)$$

where $\boldsymbol{\lambda}$ is the second-order forth-rank compliance tensor ($\boldsymbol{\lambda}_0$ is for A phase), $\boldsymbol{\varepsilon}_{\theta 0} = \boldsymbol{\alpha}_0(\theta - \theta_e)$, $\boldsymbol{\varepsilon}_{\theta k} = \boldsymbol{\alpha}_k(\theta - \theta_e)$, $\boldsymbol{\alpha}_0$ and $\boldsymbol{\alpha}_k$ are the thermal expansion tensor of A and M_k. F_{ij} is an interaction potential required to preserve the invariance of G with respect to the point group of symmetry and uniqueness of the multivariant PT at a given material point. The description of PT can now be generalized with three sets of order parameters: $\bar{0} = \{0, \eta_k = 0, 0\}$, $\bar{1} = \{0, \eta_k = 1, 0\}$ and $\bar{\eta}_k = \{0, \eta_k, 0\}$. The extremum property of the free energy density requires

$$\frac{\partial G}{\partial \eta_k} = \eta_k(\eta_k - 1)(\eta_k - \eta_{bk}) = 0 \;, \quad \eta_k = \bar{0}, \bar{1} \;, \quad (18)$$

$$\frac{\partial^2 G}{\partial \eta_k^2} \leq 0 \;, \quad \eta_k = \bar{0} \quad (A \rightarrow M_k) \quad (19)$$

$$\frac{\partial^2 G}{\partial \eta_k^2} \leq 0 \;, \quad \eta_k = \bar{1} \quad (M_k \rightarrow A) \quad (20)$$

The transformation energy associated with $A \leftrightarrow M_k$ is

$$G(\boldsymbol{\sigma}, \theta, \bar{0}) - G(\boldsymbol{\sigma}, \theta, \bar{1}) = \boldsymbol{\sigma} : \boldsymbol{\varepsilon}_{tk} - \Delta G^{\theta} \;. \quad (21)$$

Combining Eqs. (18) and (21) with similar steps described in Sec. 2, we get

$$\eta_{bk} = -6\boldsymbol{\sigma} : \boldsymbol{\varepsilon}_{tk} + 6\Delta G^{\theta} + 1/2 \quad (22)$$

Following the steps given in [7], we arrive at the symmetry preserving polynomial structure of the interaction potential

$$F_{ij} = \eta_i\eta_j(1 - \eta_i - \eta_j)\left[B\left\{(\eta_i - \eta_j)^2 - \eta_i - \eta_j\right\} + D\eta_i\eta_j\right] + \eta_i^2\eta_j^2(\eta_i Z_{ij} + \eta_j Z_{ji}) \quad (23)$$

where B, D are constants to be estimated from experiments, The transformation energy associated with $M_i \rightarrow M_j$ requires

$$G(\boldsymbol{\sigma}, \theta, \bar{\eta}_i) - G(\boldsymbol{\sigma}, \theta, \bar{\eta}_j) = \boldsymbol{\sigma} : (\boldsymbol{\varepsilon}_{tj} - \boldsymbol{\varepsilon}_{ti})$$
$$\Rightarrow \eta_{bi} - \eta_{bj} = 6\boldsymbol{\sigma} : (\boldsymbol{\varepsilon}_{tj} - \boldsymbol{\varepsilon}_{ti}) \;, \quad (24)$$

which is already satisfied through Eq. (22). The uniqueness of PT at a material point is now imposed through similar steps described in context of Eq. (8), which leads to

$$\frac{\partial}{\partial \boldsymbol{\sigma}}\left[\sum_{k=1}^{2}\sum_{j=k+1}^{3}\frac{\partial F_{kj}(\eta_k, \eta_j)}{\partial \eta_k}\right] = \sum_{k=1}^{3}\left[\boldsymbol{\varepsilon}_{tk}\frac{\partial \varphi(\eta_k)}{\partial \eta_k} + (\boldsymbol{\varepsilon}_{\theta k} - \boldsymbol{\varepsilon}_{\theta 0})\frac{\partial \varphi(\eta_k)}{\partial \eta_k} + (\boldsymbol{\lambda}_k - \boldsymbol{\lambda}_0)\frac{\partial \varphi(\eta_k)}{\partial \eta_k}\boldsymbol{\sigma}\right] \;, \quad (25)$$

The constants Z_{ij} can be estimated with the help of Eq. (25). For numerical example, we consider NiAl sample with two martensitic variants and unidirectional stress. Equal deviation of critical temperature from equilibrium temperature is assumed. The internal energy is assumed to be proportional to the temperature in the close neighbourhood of the transformation. Fig. 2(a) and (b) respectively shows the the distribution of the Gibbs free energy under applied stress of $100Mpa$ and $200MPa$. Form Fig. 1(a), it can be noted that loading upto $100MPa$ and $300K$ does not produce phase transformation, and this can also be considered a close approximation for more than one variants. As a result, G is minimum at $\eta_1 = 0$, $\eta_2 = 0$. On the other hand, martensites have already formed for loading upto $200MPa$ ($300K$) and this can be observed in Fig. 2(b) which shows global minimum at $\eta_1 = 1, \eta_2 = 1$.

With the above microscopic free energy density representation we now construct the time-dependent Ginzburg-Landau equation coupled with the thermoelasticity.

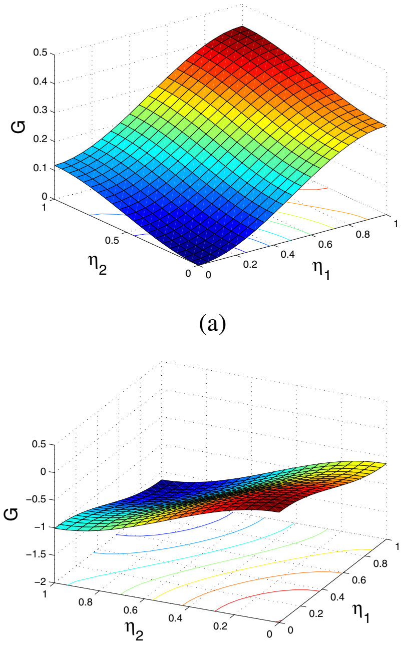

(a)

(b)

Figure 2. Variation of Gibbs free energy (plotted in 10^8 scale) at various diffused state (η_1, η_2) during stress induced transformation, $\theta_e = 215K$, $\theta = 300K$, (a) $\sigma = 100MPa$ (b) $\sigma = 200MPa$.

4. Strongly coupled dynamics of the phase transformation and coupled thermoelasticity in a rectangular NiAl bar

Our objective is now to solve the coupled field model in which the phase kinetics is governed by the Ginzburg-Landau equation

$$\frac{\partial \eta_k}{\partial t} = -\sum_{p=1}^{3} L_{kp}\left[\frac{\partial G}{\partial \eta_p} + \boldsymbol{\beta}_p : \boldsymbol{\nabla}\boldsymbol{\nabla}\eta_p\right] + \theta\ , \qquad (26)$$

where L_{kp} are positive definite kinetic coefficients, $\boldsymbol{\beta}_p$ are positive definite second rank tensor, and the macroscopic energy conservation law is governed by the heat transfer equation

$$\rho\frac{\partial \bar{G}}{\partial t} - \boldsymbol{\sigma} : \boldsymbol{\nabla}\frac{\partial \boldsymbol{u}}{\partial t} + \boldsymbol{\nabla} \cdot \boldsymbol{q} = h_\theta\ , \qquad (27)$$

and the momentum balance equation

$$\rho\frac{\partial^2 \boldsymbol{u}}{\partial t^2} = \boldsymbol{\nabla} \cdot \boldsymbol{\sigma} + \boldsymbol{f}\ , \qquad (28)$$

where

$$\bar{G} = G - \theta\frac{\partial G}{\partial \theta} \qquad (29)$$

is the internal energy, ρ is the mass density, $\boldsymbol{u}$ is the displacement vector,

$$\boldsymbol{q} = -\kappa\boldsymbol{\nabla}\theta - \alpha'\kappa\boldsymbol{\nabla}\frac{\partial \theta}{\partial t} \qquad (30)$$

is the heat flux approximated from the solution of 3D Cattaneo-Vernotte equation [10], h_θ and $\boldsymbol{f}$ are the thermal and mechanical loading, respectively. The displacement is related to the Green strain tensor as

$$\boldsymbol{\varepsilon} = \frac{1}{2}[\boldsymbol{F} : \boldsymbol{F} - \boldsymbol{I}] \qquad (31)$$

where $\boldsymbol{F}$ is the deformation gradient and $\boldsymbol{I}$ is the identity tensor.

5. Finite Element Model

Here we briefly report the FE model of the SMA dynamics and its parallel implementation aspects. We first derive the weak form of the coupled nonlinear system for general 3D configuration by introducing weighted residual of the strong form given in Eqs. (26)-(28). The appropriate choice of the admissible interpolation fields, i.e. the dependent variables $\boldsymbol{u}(x, y, z, t)$, $\theta(x, y, z, t)$ and η_k $(k = 1, \cdots, n)$, when assumed equal to the weights, leads to the weak form

$$\Pi = \Pi_{\mathrm{PT}} + \Pi_{\mathrm{thermal}} + \Pi_{\mathrm{mechanical}}\ , \qquad (32)$$

where

$$\Pi_{\mathrm{PT}} = \int_\Omega \sum_{k=1}^{n} \eta_k\left[\frac{\partial \eta_k}{\partial t} - \theta\right] d\Omega dt$$
$$+ \int_\Omega \sum_{k=1}^{n}\sum_{p=1}^{n} \eta_k\left[L_{kp}\left(\frac{\partial G}{\partial \eta_p} + \boldsymbol{\beta}_p : \boldsymbol{\nabla}\boldsymbol{\nabla}\eta_p\right)\right] d\Omega dt\ , \qquad (33)$$

$$\Pi_{\mathrm{thermal}} = \int_\Omega \theta\left[\rho\frac{\partial \bar{G}}{\partial t} - \boldsymbol{\sigma} : \boldsymbol{\nabla}\frac{\partial \boldsymbol{u}}{\partial t}\right] d\Omega dt$$
$$+ \int_\Omega \theta\left[\boldsymbol{\nabla} \cdot \left(-\kappa\boldsymbol{\nabla}\theta - \alpha'\kappa\boldsymbol{\nabla}\frac{\partial \theta}{\partial t}\right) - h_\theta\right] d\Omega dt\ , \qquad (34)$$

$$\Pi_{\mathrm{mechanical}} = \int_{t_1}^{t_2}\int_\Omega \boldsymbol{u}\left[\rho\frac{\partial^2 \boldsymbol{u}}{\partial t^2} - \boldsymbol{\nabla} \cdot \boldsymbol{\sigma} - \boldsymbol{f}\right] d\Omega dt\ . \qquad (35)$$

Integrating Eqs. (33)-(35) by parts and applying divergence theorem such that the orders of differentiation are evenly distributed among the weights and the terms within the brackets, we get the weak form as sum of three parts:

1. the terms integrable in (Ω, t)
2. the terms integrable in t but prescribed at spatial boundary (Γ) and

3. the terms integrable in Ω but prescribed at $t = t_1$.

Rewriting all the tensors as matrices and applying first variation of the weak functional (Π), we get the global equilibrium equation

$$\delta\Pi = 0 \ , \tag{36}$$

in which the variation over (1) gives the homogeneous state equation in matrix-vector form and body force, (2) gives the natnaturalundary term (forcing vector) and (3) gives the initial condition (initial state vector).

In our study we consider the vector of interpolation field variables as

$$\boldsymbol{v} = \{u_1\ u_2\ u_3\ \theta\ \eta_1\ , \cdots\ , \eta_n\}^T \ , \tag{37}$$

where according to our previous discussion, u_i are thee displacement components, η_k are the order parameters for kth variant of phases in the microscopic scale. The superscript e indicates FE nodal variable. In the mesoscopic scale all the η_k take part in the FE integrations depending on the description of the phase at each integration point. The generic vector of interpolation is expressed in the following form

$$\{u_1\ u_2\ u_3\}^T = \boldsymbol{N}_u \boldsymbol{v}^e \ , \quad \theta = \boldsymbol{N}_\theta \boldsymbol{v}^e \ , \quad \eta = \boldsymbol{N}_\eta \boldsymbol{v}^e \ , \tag{38}$$

where $\boldsymbol{N}_u$, $\boldsymbol{N}_\theta$ and $\boldsymbol{N}_\eta$ are the FE interpolation functions for the displacement, the temperature and the order parameters, respectively. Linear interpolation functions are used for the present study. The strain displacement relation has linear and nonlinear contributions. In the total Lagrangian framework, we express the strain at any step of iteration at time $t + \Delta t$ as

$$\boldsymbol{\varepsilon} = \boldsymbol{B}\boldsymbol{v}^e + \boldsymbol{B}_L(\boldsymbol{u}^t)\boldsymbol{v}^e \ , \tag{39}$$

where $\boldsymbol{B}$ is the linear strain-displacement matrix and $\boldsymbol{B}_L$ is the non-linear train-displacement matrix as function of the displacement ($\boldsymbol{u}^t$) obtained from the previous converged time step at t. Similarly, the transformation strain is expressed as

$$\boldsymbol{\varepsilon}_t \varphi(\eta_k) = \boldsymbol{\varepsilon}_t \bar{\boldsymbol{N}}_\varphi(\eta_k^t)\boldsymbol{v}^e \ , \tag{40}$$

where $\bar{\boldsymbol{N}}_\varphi$ is function of the order parameter (η_k^t) from the previous converged time step at t. The vector of stresses is expressed as

$$\boldsymbol{\sigma} = \boldsymbol{C}\left(\boldsymbol{B} + \boldsymbol{B}_L\right)\boldsymbol{v}^e - \boldsymbol{C}\boldsymbol{\varepsilon}_t\bar{\boldsymbol{N}}_\varphi\boldsymbol{v}^e \ , \tag{41}$$

where $\boldsymbol{C} = \boldsymbol{\lambda}^{-1}$ is the stiffness matrix. Also,

$$\Delta G^\theta = (\Delta s_e - \Delta c)\theta_e + (-\Delta s_e + \Delta c)\boldsymbol{N}_\theta\boldsymbol{v}^e - \Delta c\bar{\boldsymbol{N}}_\theta(\theta^t)\boldsymbol{v}^e \ , \tag{42}$$

where $\bar{\boldsymbol{N}}_\theta$ is function of temperature (θ^t) from the previous converged time step at t. Eq. (36) is now expanded with the help of Eqs. (37)-(42), which finally gives the global equilibrium equations in matrix-vector form at a time step $t + \Delta t$ as

$$\boldsymbol{A}_1\ddot{\boldsymbol{v}}^e + \boldsymbol{A}_2\dot{\boldsymbol{v}}^e + \boldsymbol{A}_3\boldsymbol{v}^e = \boldsymbol{F} + \boldsymbol{R}(\boldsymbol{v}^{et}) \ , \tag{43}$$

and the initial condition as

$$\boldsymbol{J}_1\boldsymbol{v}^e = \boldsymbol{Q}_1 \ , \quad \boldsymbol{J}_2\dot{\boldsymbol{v}}^e = \boldsymbol{Q}_2 \ . \tag{44}$$

Newton iteration is performed to obtain convergence in $\boldsymbol{v}^e$ at each time step. The increments in $\boldsymbol{u}^e$, θ and η_k are obtained individually after applying Newmark's time integration scheme on Eq. (43) and then by evaluating the energy estimate based on Eq. (32) and using the tangent matrices from the previous converged time step at t. At this step, one needs to compute the Jacobian of the element-wise estimate Π and perform inversion of this Jacobian matrix for each element at each step of iteration. This procedure can ensures faster convergence as compared to constructing the global estimate Π and obtain the increments for all the nodal variables simultaneously.

At each time step, the time discretized form of Eq. (43) is finally given by the matrix-vector equation

$$\boldsymbol{A}\boldsymbol{v}^e = \boldsymbol{b} \ . \tag{45}$$

Due to the coupled and non-linear nature of the weak form in Eqs. (32)-(35), it is observed that the system matrices $[A_1]$, $[A_2]$ and $[A_3]$ are in general not symmetric. Hence the matrix $\boldsymbol{A}$ in Eq. (45) is also not symmetric. But they are banded because of usual FE discretization of the spatial domain. We use wave-front based bandwidth minimizer within the time integration loop.

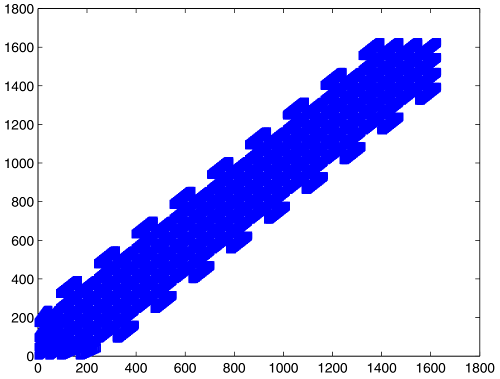

Figure 3. Structure of effective stiffness matrix $[A_3]$ for a $10 \times 10 \times 1$ element discretization using 8-node tetrahedral elements with 7-dof/node.

Fig. 3 shows the banded structure of the FE system for a $10 \times 10 \times 1$ element discretization for a shape memory alloy thin film. Although, the resulting system size is significant, a typical mesh to satisfy the convergence requirement for microstructural evolution can be many times this size. Another important note is that the interpolation field variables are not used in non-dimensional form in the present FE model, since such a non-dimensionalized form is difficult to obtain for a general dynamic case (see Ref. [8]). Hence, it is obvious that the system matrix $\boldsymbol{A}$ must be preconditioned before it can be solved with required accuracy. One of the choice here is to reorder the variables in three groups (i.e. $\{u\}^e$, $\{\theta\}^e$ and $\{\eta\}^e$). But then the main difficulty is due to the loss of bandedness. Reported studies [5] have shown that for certain cases of reordering, certain degree of parallelism can be achieved by using preconditioner based on incomplete factorization. Among other studies, unpreconditioned conjugate gradient (CG) method [1, 2] has been reported, which can be implemented in parallel. In the present work we propose a parallel scheme for the banded system in Eq. (45) using Jacobi preconditioner and standard PCG solver. The approach is similar to one recently reported in [12] which was successfully tested with the coupled nonlinear Belousov-Zhavotinskii reaction-diffusion model. The detail aspects of the parallelism and communication overlap that are achieved during the matrix-vector multiplication in PCG iteration can be found in [12] and the references therein. In addition to this, future research may be directed to the assembly of matrix $\mathbf{A}$ in parallel and attempt an optimal load balancing. In the present work we base our computation using portable message passing interface (MPICH) in distributed memory environment.

6. Concluding remarks

A coupled nonlinear dynamic model of phase transformations in three-dimensional SMA based on microscopic Landau theory is developed and implemented in a finite element framework in this paper. Essential properties of the $A \leftrightarrow M_j$ as well as $M_j \leftrightarrow M_i$ phase transformations are recovered using consistent steps, which eliminates the problem of non-uniqueness of energy partitioning during phase transformation and relaxes the over-sensitivity of the free energy due to many unknown material constants in previously reported models. A variationally formulated finite element model is developed for intensive numerical simulation. Newmark's time integration is adopted. The steps involved in consistent discretization and iteration of the vector of nodal variables are discussed.

References

[1] C. Aykanat, F. Ozguner, and D. S. Scott. Vectorization and parallelization of the conjugate gradient algorithm on hypercube connected vector processors. *Microprocessing and Microprogramming*, 1990:67–82, 29.

[2] A. T. Chronopoulos and C. W. Gear. S-step iterative method for symmetric linear systems. *J. Comput. Appl. Math.*, 25:153–168, 1989.

[3] F. Falk and P. Kanopka. Three-dimensional landau theory describing the martenstic phase transformation of shape - memory alloys. *J. Phys.: Condens. Matter*, 2:61–77, 1990.

[4] T. Ichitsubo, K. Tanaka, M. Koiwa, and Y. Yamazaki. Kinetics of cubic to tetragonal transformation under external field by the time-dependent ginzburg-landau approach. *Physical Rev. B*, 62:5435, 2000.

[5] M. T. Jones and P. E. Plassmann. A parallel graph coloring heuristic. *SIAM J. Sci. Stat. Comput.*, 14:654–669, 1993.

[6] V. Levitas and D. L. Preston. Three-dimensional landau theory for multivariant stress-induced martensitic phase transformations. i. austenite ↔ martensite. *Physical Rev. B*, 66:134206, 2002.

[7] V. I. Levitas and D. L. Preston. Three-dimensional landau theory for multivariant stress-induced martensitic phase transformations. ii. multivariant phase transformations and stress space analysis. *Physical Rev. B*, 66:134207, 2002.

[8] V. I. Levitas and D. L. Preston. Three-dimensional landau theory for multivariant stress-induced martensitic phase transformations. iii. alternative potentials, critical nuclei, kink solutions, and dislocation theory. *Physical Rev. B*, 68:134201, 2003.

[9] P. Matus, R. V. N. Melnik, L. Wang, and I. Rybak. Application of fully conservative schemes in nonlinear thermoelasticity: modelling shape memory materials. *Mathematics and Computers in Simulation*, 65:489–510, 2004.

[10] R. V. N. Melnik, A. J. Roberts, and K. A. Thomas. Computing dynamics of copper-based shape memory alloys via center manifold reduction of 3d models. *Computational Material Science*, 18:255–268, 2000.

[11] C. Niclaeys, T. Benzineb, and E. Patoor. Finite elemet simulation of a multicrystal in shape memory alloy. *J. Phys. IV France*, 115:375–382, 2004.

[12] E. M. Ortigosa, L. F. Romero, and J. I. Ramos. Parallel scheduling of the pcg method for banded matrices rising from fdm/fem. *J. Parallel Distrib. Comput.*, 63:1243–1256, 2003.

[13] B. Peultier, T. Benzineb, and E. Patoor. Modelling of the martensitic phase transformation for finite element computation. *J. Phys. IV France*, 115:351–359, 2004.

[14] Y. H. S. Fu and I. Muller. Thermodynamics of pseudoelasticity - an analytical approach. *Acta Mechanica*, 99:1–19, 1993.

1550-5243/05 $20.00 © 2005 **IEEE**

Table of Contents

HPCS 2005

Preface...ix
Steering Committee...xi
Scientific Committee...xi
Local Organizing Committe...xii

Applications and MISC

Distributed Artificial Neural Network Architectures...2
D. Calvert and J. Guan

Benchmarking of a 3D, Unstructured, Finite Volume Code of Incompressible Navier-Stokes equation on a Cluster of Distributed-Memory Computers...11
S. Karimian and A. Straatman

A Meta-Software System for the Discovery of Hadamard Matrices...17
I. Kotsireas and G. Pinheiro

Quintic Spline Based Computational Scheme for Singularly Perturbed Convection-Diffusion Problems...24
R. Bawa and S. Natesan

The Study and Implementation of the Multigrid Algorithm for the 3-D Transport Difference Equation...29
Y. Shulin and S. Weidong

Astrophysics

The Analysis of Large Order Bessel Functions in Gravitational Wave Signals from Pulsars...34
F. Chishtie, S. Valluri, K. Rao, D. Sikorski, and T. Williams

The Effects of Stellar Winds on the Envelope Masses of Cooling Low-Mass Dwarfs...42
L. Nelson and E. Dubeau

Biomedical

High Performance Derivative-Free Optimization Applied to Biomedical Image Registration...50
M. Wachowiak and T. Peters

CS and HPC Tools

A Customizable Component for Low-Level Communication Software...58
T. Santos and A. Frohlich

Hpcbench — A Linux-Based Network Benchmark for High Performance Networks...65
B. Huang, M. Bauer, and M. Katchabaw

A Replacement Policy to Save Energy for Data Cache...72
S. Musalappa, S. Sundaram, and Y. Chu

Applying Fault-Tolerant Solutions of Circulant Graphs to Meshes and Hypercubes...76
S. Lou and A. Farrag

B-Rep Based Parallel Machining Simulation...83
R. Fleisig and A. Spence

Exploiting Multithreaded Programming on Cluster Architectures...90
O. Cordeiro, D. Peranconi, L. Real, E. Dall'Agnol, and G. Cavalheiro

Exploring Parallel Programming Knowledge in the Novice 97
R. Eccles, B. Nonneck, and D. Stacey

A Fully Parallel and Scalable Implementation of a Hopfield Neural Network on the SHARC-NET Supercomputer 103
E. Sykes and A. Mirkovic

The HPCVL Working Template: A Tool for High-Performance Programming 110
G. Liu, H. Schmider, and K. Edgecombe

High Performance Constraint Satisfaction Problem Solving: State-Recomputation versus State-Copying 117
J. Yang and S. Goodwin

A Load Balancing Approach Based on a Genetic Machine Learning Algorithm 124
M. Dantas and A. Pinto

Message-Passing and Shared-Data Programming Models — Wish vs. Reality 131
A. Sodan

This paper was withdrawn by the author 140

Scheduling Based on the Impact over Process Communication of Parallel Applications 149
R. Ishii, R. de Mello, L. Senger, M. Santana, and R. Santana

Software Engineering Issues for Small-Scale Parallelism 156
R. Eccles and D. Stacey

Topology Reconfiguration Mechanism for Traffic Engineering in WDM Optical Network 161
B. Gillani, R. Kent, and A. Aggarwal

Financial Mathematics

Parallel Lattice Implementation for Option Pricing under Mixed State-Dependent Volatility Models 170
G. Campolieti and R. Makarov

Parallel Algorithm for Pricing American Asian Options with Multi-Dimensional Assets 177
K. Huang and R. Thulasiram

Grid Computing

An Adaptive Generalized Scheduler for Grid Applications 188
A. Aggarwal and R. Kent

Comparison of Advanced Authorisation Infrastructures for Grid Computing 195
A. Stell, R. Sinnott, and J. Watt

Computational Science on the Grid: From Testbeds to Production 202
G. Mateescu and J.-C. Côté

Genetic Algorithm Based Scheduler for Computational Grids 209
M. Aggarwal, R. Kent, and A. Ngom

Grid-Enabling the Global Geodynamics Project: The Introduction of an XML-Based Data Model 216
L. Lumb and K. Aldridge

Using Ontology for Description of Grid Resources 223
A. Pernas and M. Dantas

Data Agnostic Resource Scheduling in the Grid 230
G. Hayward and L Lumb

Life Sciences

Recognizing Patterns in High-Dimensional Data: Automated Histogram Filtering for Protein Structure Elucidation 238
J. Imada, P. Chapman, and S. Rothstein

Simulation of Electrical Conduction in Cardiac Tissue on High Performance Computers 244
T. Almas, Z. Tesfaye, and I. Donn

A Lightweight, Scalable Grid Computing Framework for Parallel Bioinformatics Applications 251
H. De Sterck, R. Markel, and R. Knight

Materials

Parallel Computing for Sheet Metal Strain Analysis 260
H.-L. Chan, A. Spence, and M. Sklad

Computational Modeling of Coupled Dynamic Phase Transformations in Shape Memory Alloys 267
D. Mahapatra and R. Melnik

Mathematical Modelling

The First Hundred Years of Numerical Weather Prediction 276
G. Brunet

Netzwerk: Migration of a Packet-Switching Network Simulation Environment from MS Windows PC to Linux PC and to HPC 280
A. Lawniczak, A. Gerisch, K. Maxie, and B. Di Stefano

Physics

Advanced Modeling of Quantum Well Semiconductor Lasers Based on Wigner Function Approach 288
M. Wartak and P. Weetman

Parallel Implementation of Density Functional Theory within the Real Space Pseudopotential Approach 295
E. Kadantsev and M. Scott

The 3rd Annual Open Source Cluster Application Resources Symposium

OSCAR 2005

A Wireless Monitoring Approach for a HA-OSCAR Cluster Environment 302
M. Dantas and C. Rista

A SMS Tool for Alerts and Monitoring of a High Availability Cluster Envioronment 307
M. Dantas and R. Baggio

OSCAR on Debian: The EDF Experience 312
G. Vallée, J.-Y. Berthou, H. Prisker, and D. Leprince

SSI-OSCAR: A Cluster Distribution for High Performance Computing Using a Single System Image 319
G. Vallée, S. Scott, C. Morin, J.-Y. Berthou, and H. Prisker

Revamping the OSCAR Database: A Flexible Approach to Cluster Configuration Data Management 326
D. Kim, J. Squyres, and A. Lumsdaine

Grid-Aware HA-OSCAR 333
K. Limaye, B. Leangsuksun, V. Munganuru, Z. Greenwood, S. Scott, R. Libby, and K. Chanchio

Virtualization of Linux Based Computers: The Linux-VServer Project 340
B. des Ligneris

Automated OSCAR Testing with Linux-VServers 347
F. Camargos and B. des Ligneris

OSCAR Meta-Package System 353
J. Mugler, T. Naughton, and S. Scott

Author Index 361